Assessment and Mitigation of Seismic Risk at the Urban Scale: An Application to the Historic City Center of Leiria, Portugal

Anna Blyth[1], Beatrice Di Napoli[1], Francesco Parisse[1], Zahir Namourah[1], Elsa Anglade[1,2], Anna-Maria Giatreli[1],

Hugo Rodrigues[3], Tiago Miguel Ferreira[1,*]

[1]ISISE, Institute for Science and Innovation for Bio-Sustainability (IB-S), Department of Civil Engineering, University of Minho, Portugal

[2]Département Génie Civil, Ecole Normal Supérieure de Paris-Saclay, France

[3]RISCO, Department of Civil Engineering, Polytechnic Institute of Leiria, Portugal

*Corresponding author: tmferreira@civil.uminho.pt

Abstract: The implementation of a culture of seismic risk preparedness is becoming increasingly critical in Europe as the building stock ages and the awareness about seismic risk rises. In this context, the assessment of the seismic vulnerability of existing buildings, followed by the implementation of appropriate retrofitting solutions, can help to substantially reduce the levels of physical damage and economic impact of future events. The central region of Portugal is particularly susceptible to large seismic events and is characterized by the prevalence of historic masonry buildings. This work aims to validate assessment methods for the risk of historical city centers in order to propose management strategies for municipalities and assess the economic impact of large-scale seismic retrofitting. To do this, an application of these methods was performed on the historical city center of Leiria. An in-depth inspection was performed of the entire center and the results were compiled into a database. Using an index-based seismic vulnerability assessment approach, a vulnerability assessment was made for each building. Based on vulnerability and predicted damage, estimates of human and economic losses were made for the city center before and after retrofitting to justify interventions on a broad scale.

Keywords: Risk Management, Seismic Vulnerability Assessment, Historic Centers, Masonry Buildings, Retrofitting Strategies.

1 Introduction

The cultural value of historical city centers can be considered the result of long-term processes dealing with ethnological, political, economic, architectural and artistic values (Vicente et al. 2015). Their unique identity should be recognized and characterized by analyzing the urban morphology and by understanding the history and cultural background. Any potential intervention should be based on this knowledge and be a result of a systematic method of assessment and recording that ensures compatibility during the urban regeneration process. A strategic and standardized methodology with a large scale, sustainable, and multidisciplinary approach for defining outlines and procedures of intervention is required even though this framework is likely to have some singularities since each case is unique (Ferreira et al. 2015). The vulnerabilities of historical city centers are still not completely understood by governments. The implementation of risk policy is limited even though the scientific community has

1

43 increased its research on this issue providing guidelines, methodologies, technologies, and tools to
44 evaluate and monitor the existing framework and predict potential scenarios (Ferreira et al. 2017a).
45 Although some methodologies are more accurate in terms of results, they may be not economically
46 viable, so simplified seismic vulnerability assessment methods can play an important role in developing
47 vulnerability scenarios at urban or building scales (Ferreira et al. 2017a). This article is aimed at
48 evaluating the vulnerability of the historical city center of Leiria, Portugal, by using the vulnerability
49 index methodology developed by Vicente et al. (2011) based on the Italian GNDT II level approach
50 (GNDT 1994), with the quantification of the uncertainty through the introduction of the concept of
51 parameter confidence factor. In an attempt to account for the uncertainty associated with the evaluation,
52 this confidence factor opens the door to future advances on the quantification of that uncertainty on the
53 risk assessment results. The present work aims to provide quantitative data about the risks associated
54 with seismicity of Leiria, guiding the municipality through the making of informed decisions about a
55 risk management plan and retrofitting strategies.

56 2 The Historical City Center of Leiria

57 2.1 Overview of the case study

58 Leiria, located in central Portugal, is one of the main cities between Coimbra and Lisbon. It is widely
59 known that the Portugal mainland is a slow seismic deforming region, where the interaction between
60 the African and Eurasian plates can be responsible for large earthquakes. In the last century, the region
61 has experienced at least 116 earthquakes with intensities equal or larger than III on the EMS-98
62 macroseismic intensity scale (Teves-Costa et al. 2019). The most notable for the seismic history of
63 Portugal is the 1755 Lisbon earthquake (8.5 ± 0.3 Mw) that caused great damage in the Algarve and
64 Lisbon regions as well as in Leiria (Carvalho and Aveleira n.d.). According to maximum intensity maps
65 (MIM) available for Portugal mainland, intensity VII or VIII can be identified as representative of the
66 seismicity of the city (Teves-Costa et al. 2019). Thus, Leiria is at acute risk of destructive earthquakes
67 and should prepare adequate risk management strategies.

68 The foundation of the city can be traced back to 1135 when D. Afonso Henriques built its castle (Mattoso
69 1985). Since then, it has flourished thanks to its position first as an outpost to the Moorish domains and
70 later as a commercial hub. The urban configuration developed in relation to the castle and the two
71 landmarks of the mains square and the cathedral. Its layout is defined by the fundamental axis of Rua
72 Direita and related streets branching perpendicularly. The present work focused on a limited portion
73 (45,000 m^2) of the city corresponding to the historical center that, in preparation for fieldwork, was
74 divided into three zones (Figure 1), and each building was identified with a unique identification code.

75

76 Figure 1. Case study zones, adapted from Anglade et al. (2020)

77 Among the analyzed buildings, 49.7% were multi familiar, 38.2% single familiar, 32.5% with mixed
78 use, and 39.5% of the buildings were unoccupied. According to a socio-demographic census carried by

2

79　the municipality of Leiria there are 315 residents in the city center divided into the three zones (Dinis
80　2006), see Table 1.

81

Table 1. Demographic data presented by zone and by age groups (Dinis 2006)

Zone	Residents by Age					
	Age 0-4	Age 5-13	Age 13-24	Age 25-65	Age >65	Total
Zone 1	6	8	9	67	30	120
Zone 2	3	7	13	50	22	95
Zone 3	0	3	5	58	34	100
Total	9	18	27	175	86	315

82　## 2.2　Building characterization

83　The area is composed of 232 buildings divided into three main typologies: concrete (RC) buildings,
84　31.1% of the analyzed building stock; mixed structures, 7.9%; and masonry buildings, 61%, which
85　represent the main focus of this work. RC buildings fall outside the scope of the study and are omitted
86　from the data.

87　### 2.2.1　Geometrical features

88　The study area is composed of a fairly homogeneous building stock with common features that were
89　easily identifiable during fieldwork.　The buildings are generally part of an aggregate, and they tend to
90　be of 3-4 stories and regular in both plan configuration and height. The façade layout characterization
91　is also notable, as it has a great influence on the shear resistance and in-plane response of the façade
92　walls. The façade openings were found to be of notable size and fairly regular in layout for façades
93　facing the main streets and squares, see Figure 2 (a) and (b), while in secondary streets they present a less
94　regular configuration and are smaller in size, Figure 2 (c). In some cases, sources of irregularity both in
95　plan and elevation were introduced by later interventions carried out on the buildings, such as additions,
96　super elevations, creation of larger openings at the ground floors, floor slab replacements, etc.
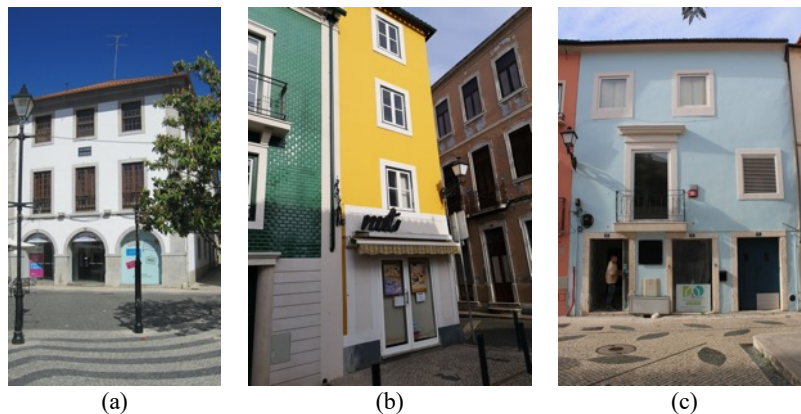

(a)　　　　　　　　(b)　　　　　　　　(c)

Figure 2. Regular big openings facing of a building facing the cathedral's square (a), a minor
square (b) and irregular size and layout openings of a secondary street (c)

97　### 2.2.2　Materials and connections

98　External inspections were used to evaluate the quality of masonry because deterioration of the external
99　renders allowed for direct observation of the material underneath. The external walls of the buildings
100　are mainly composed of stone masonry, usually limestone units of different sizes sometimes mixed with
101　units of other materials, e.g. clay bricks, marlstones, etc. The units' arrangement has sub-horizontal
102　mortar joints, but the alignment of the vertical joints does not indicate a good quality masonry (Borri
103　al. 2015). In addition, there is large variability in the size and shape of the units, Figure 3. The walls'
104　thicknesses range from 0.4 m to 1.0 m with an average of 0.7 m and are a three-leaf arrangement with
105　weak inner filling and lack of connections. The mechanical properties of the masonry were identified

3

106 according to the *"Masonry of roughhewed stones"* category defined in the Italian Codes (Circolare 21
107 gennaio 2019 n. 7 C.S.LL.PP. 2019) and confirmed by flat jack tests performed by Pinheiro et al. (2017).

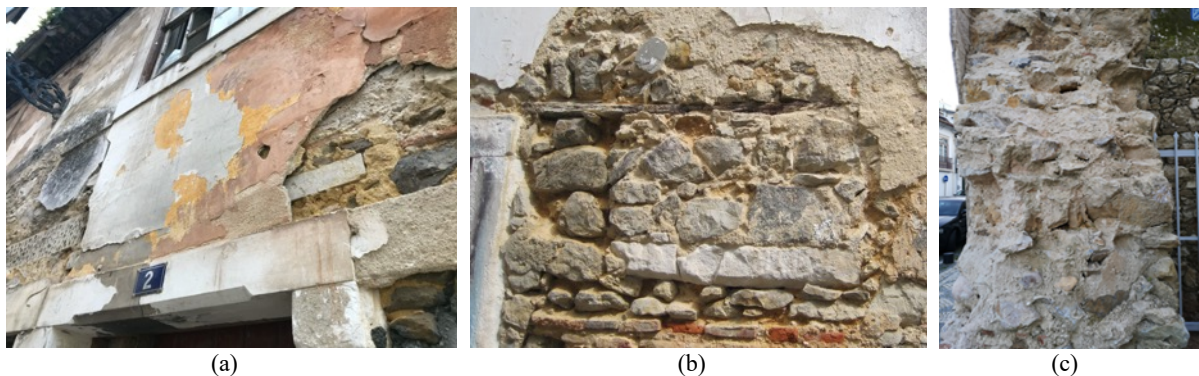|		
(a)	(b)	(c)

Figure 3. Rubble stone masonry with other material units: sub-horizontal arrangement (a, b) and cross section (c) of some masonry walls in Leiria

108 Good wall-to-wall connection was often evidenced by the presence of large stones in the façade corners,
109 Figure 4 (a). Thus, when this feature was detected, good quality of the wall-to-wall connection was
110 assumed for the building. If this was not observed, a bad quality connection and improper interlocking
111 was assumed. This assumption was supported by observations of large vertical and diagonal cracks, an
112 indication of a poor connection between the internal and external walls that allows for independent
113 behavior and rotation of the façade walls, Figure 4 (b) and (c).

(a)	(b)

114 Figure 4. Bad quality connections between orthogonal walls evidenced by diagonal cracks on internal walls (a)
115 and by detachment cracks on the corners (b)
116

117 Three floor types were observed in the study area: concrete slabs, metallic structures, and timber floors.
118 The first two typologies were observed in just a few cases in buildings that were recently restored, while
119 the third type was found in the majority of buildings. The timber floors are composed of pine beams
120 directly supported by the bearing wall or by a primary order of timber beams, Figure 5 (a). No tie rods
121 or metallic elements were observed to improve connections between the floor and walls. Thus, a
122 conservative assumption was made when information about the floor was not available: the presence of
123 a flexible timber floor with weak connections to the walls and no presence of tie rods was assumed.

124 Few roofing systems were accessible during the fieldwork. However, all of the roofs inspected consisted
125 of timber truss elements. In some cases, half trusses were observed, but in most cases king post trusses
126 or simple trusses were used, Figure 5 (b). Additionally, in all the inspected roofs, the truss structure was
127 connected to the walls through a dormant beam extending all along the perimeter with load distribution
128 and tying function, Figure 5 (c). This beam is a mixed masonry-timber element that indicates that the

4

129 roof weight and thrust are properly distributed to the perimeter walls and a good connection between
130 walls and roof is assured. It was assumed that inaccessible roofs are similar to the ones inspected. These
131 assumptions, namely the non-impulsive nature of the roof and the presence of a perimeter ribbon, might
132 lead to an underestimation of the vulnerability of the buildings to the roofing system interaction.
133 However, the assumptions made are supported by observations made in the field inspections and by the
134 knowledge of the traditional construction techniques of the area. For these reasons the assumptions made
135 are considered sufficiently cautious.

| (a) | (b) | (c) |

Figure 5. Example of a two-order timber floor with connection to the perimeter wall (a), timber king post truss
of a roof (b), mixed masonry-timber perimeter ribbon of the roof (c)

136 **3   Inspection procedure and database**

137 All the buildings in the study area were assessed on site to collect the required data for the computation
138 of the vulnerability indices by using a detailed checklist built for this purpose. It was developed to
139 evaluate each construction element of the relevant (non-reinforced concrete) buildings based on
140 scientific knowledge and experience with the chosen methods and site of the engineers conducting the
141 evaluations. The checklist was adapted from a Portuguese interpretation of the Italian *Gruppo nazionale*
142 *per la difesa dai terremoti* (GNDT) checklist for seismic vulnerability evaluations of the building stock
143 in Italy, thus combining expertise on seismic evaluation and regional construction methods (GNDT
144 2003; dos Santos Gomes 2016). In addition, the necessary data were identified from studies performed
145 by Vicente et al. (2011) and Ferreira (2010) as those most important to collect for the computation of
146 the vulnerability index values. Any necessary information that could not be obtained from a ground-
147 level visual inspection alone was left blank on the checklist to be completed with another data source
148 (i.e. Google Maps, Google Earth, or the municipality site map) or expert assumption. The data contained
149 in the checklists was manually inputted into a spreadsheet database to create a digital record and to
150 automate some later steps of the work. In fact, the vulnerability index tool spreadsheet automatically
151 pulled information from the database without needing to re-enter information manually. It was only
152 necessary to manually enter a small amount of the information required that was not possible to gather
153 directly or that was not related to singular buildings.

154 Once all the indices and seismic vulnerability indicators for each building were computed, e.g. mean
155 damage grade, probability of collapse, probability of unusability, etc., the results were plotted spatially
156 with a general planning tool. In many cases, without the use of a representative approach that allows the
157 technicians and the decision makers to acquire a global view of the area and of the results of the
158 assessment, the risk management effectiveness can be compromised (Ferreira et al. 2013). For this
159 reason, a multi-purpose tool connected to a relational database within a GIS environment was used in
160 this work. The GIS application software (*QGIS 3.4.4 – Madeira)* represents each building by its plan
161 footprint to plot the results of the assessment. All the buildings in the study area were inspected from
162 the exterior; of these, 6.2% were inspected from the interior as well, see Figure 6. Exterior inspections
163 were performed from ground level and at each accessible façade on the building. Approximately 70%
164 of the data on the checklist could be obtained from an exterior inspection alone. When an inside

5

165 inspection was possible, more precise information regarding the floor slabs and the roofing system was
166 gathered along with more information regarding the state of conservation. In most cases the type of
167 inspection carried out did not impose a significant change in the vulnerability index. However, the
168 information gathered during the internal inspections was used as a representative sample of the
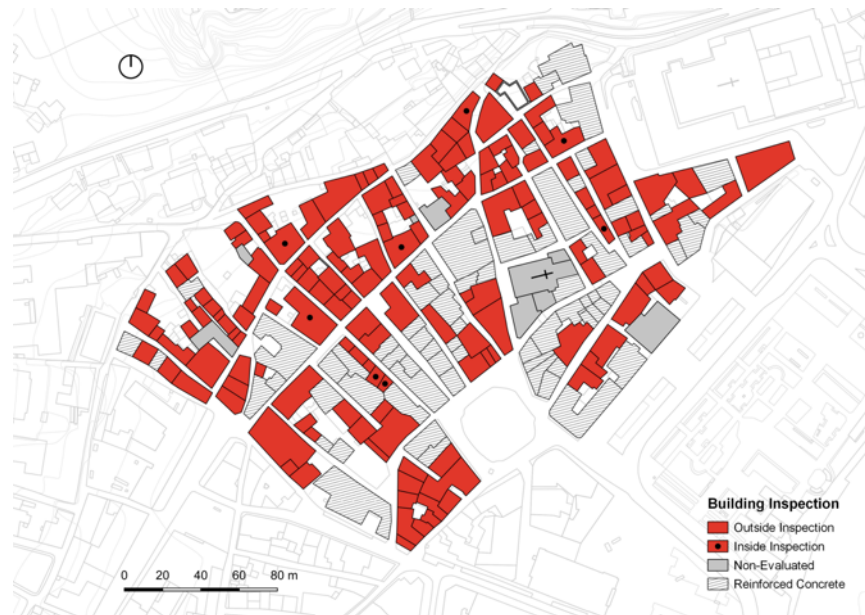169 remaining building stock.

Figure 6. Map with the type of inspection, adapted from Anglade et al. (2020)

170   4   Vulnerability index methodology

171 The vulnerability assessment was carried out using a hybrid approach based on the GNDT II level
172 approach for the masonry buildings (GNDT 2003). The method was proposed by Vicente et al. (2011)
173 and developed by other authors (Ferreira 2010). It aims to estimate possible losses and post-seismic
174 scenarios through a simplified assessment that utilizes post-seismic damage observations and survey
175 data on the elements that define building damage (Maio et al. 2016). The method has been successfully
176 adapted to the Portuguese historical building environment (Ferreira et al. 2017a; Maio et al. 2016;
177 Vicente et al. 2011) and is calibrated according to damage data collected for the magnitude VII
178 earthquake that struck the Azores archipelago in 1998 (Ferreira et al. 2017a). It is worth noting in this
179 regard that, although the method is not specifically calibrated for this case study (which would be
180 impossible since no damage data is available), the fact that it has been calibrated based a similar building
181 typology, with similar constructive and geometrical features, allows to assume the validity of the results.
182 As explained in the following, possible differences in the mechanical characteristics of the structural
183 elements are considered and controlled by the method.

184 The method evaluates 14 parameters that affect the seismic performance of the building stock. A
185 vulnerability class (c_{vi}) is assigned to these parameters with increasing vulnerability: A, B, C, and D
186 and a weight (p_i) is given ranging from 0.5 for the least important parameters to 2.5 for those considered
187 most important (Table 2). The parameters are used evaluate a single building in an aggregate and are
188 organized into four groups: structural building system, irregularities and interaction, floor slabs and roof,
189 conservation status and other elements. A total vulnerability index I_v is calculated with Equation (1) by
190 computing the weighted sum of the parameters multiplied by their specific weight assigned as a meaning
191 of importance in the definition of seismic response. The total vulnerability index takes on an integer
192 value in the range between 0 and 750; it is then normalized to a global vulnerability index (I_v) ranging
193 between 0 and 100.

6

$$I_v = \sum_{i=1}^{14} c_{vi} \times p_i \qquad (1)$$

194 Each parameter was evaluated based on expert opinion but has inherent uncertainty. To account for this,
195 confidence levels were evaluated and are presented in Section 5.2.

196 Table 2. Vulnerability index associated parameters, classes and post-calibration weights p_i (Ferreira et al. 2017a)

Parameters	Class, C_{vi}				Weight	Relative weight
	A	B	C	D	p_i	
Group 1. Structural building system						
P1. Type of the resisting system	0	5	20	50	2.50	
P2. Quality of the resisting system	0	5	20	50	2.50	
P3. Conventional strength	0	5	20	50	1.00	50/100
P4. Maximum distance between the walls	0	5	20	50	0.50	
P5. Number of floors	0	5	20	50	0.50	
P6. Location and soil condition	0	5	20	50	0.50	
Group 2. Irregularities and interaction						
P7. Aggregate position and interaction	0	5	20	50	1.50	
P8. Plan configuration	0	5	20	50	0.50	20/100
P9. Height regularity	0	5	20	50	0.50	
P10. Wall facade openings and alignments	0	5	20	50	0.50	
Group 3. Floor slabs and roofs						
P11. Horizontal diaphragms	0	5	20	50	0.75	18/100
P12. Roofing system	0	5	20	50	2.00	
Group 4. Conservation status and other elements						
P13. Fragilities and conservation status	0	5	20	50	1.00	12/100
P14. Non-structural elements	0	5	20	50	0.75	

197 **5   Vulnerability assessment of the Historical Center of Leiria**

198 **5.1   Assessment of parameters**

199 The compilation of the database and analysis of the parameters yields the parameter class distribution
200 shown in Figure 7. Of these, P1, P2, P7, and P12 were found to be the most influential and given a
201 weight of 1.5 or greater (Table 2). Parameters P3, P11, and P13 are also notable with weights of 1.0; P1,
202 P2, P3, P11, P12, and P13 are the target of the retrofitting strategies presented in Section 6. The position
203 of a building within its aggregate (P7) is fixed and thus unaffected by retrofitting.
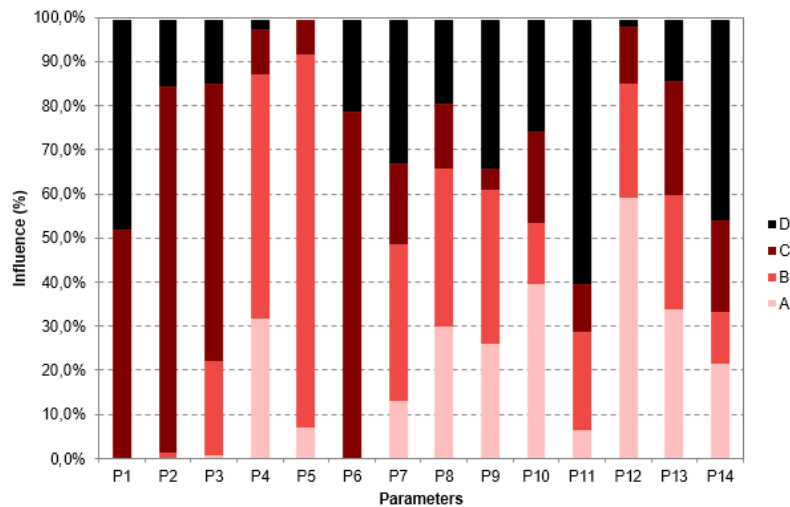

204
205   Figure 7. Vulnerability class distribution of each parameter

7

5.2   Parameter confidence factors

The inherent uncertainty of the parameters necessitates an evaluation of the confidence in the data and the error accumulated during the gathering procedure. The propagation of error should be considered when evaluating the vulnerability index values. The present work attributed confidence classes to the parameters according to Vicente (2008), defined on the basis of the quality of the information gathered. A quantitative range of uncertainty from 0%, total confidence, to 100%, total uncertainty, was assigned to each confidence level listed in Table 3.

Two approaches were used for the uncertainty grade computation: an assumption based on expert opinion when the evaluation of a specific parameter consisted of a single data type or of a simplified assessment (P2, P5, P7, P8, P10, P13 and P14); or a combination of the uncertainty grades associated with the data used (P1, P3, P4, P6, P11 and P12). Thus, the factors applied as uncertainty levels can also be considered as an estimation of the error accumulated during data recording and assumption. A global confidence level for a single building cannot be computed because a summation would lead to overlapping sources of uncertainty (i.e. the presence of tie rods influences both parameters P1 and P12). Therefore, only the confidence levels related to a single parameter are provided. Still the results of this methodology can be used to discuss the reliability of the method applied. Table 3 presents the mean confidence classes calculated for each parameter with the associated graph shown in Figure 8.

Table 3. Average confidence classes for each parameter

Parameter	Strategy	Average uncertainty	Average confidence class
P1	Combined	38.2%	M
P2	Assigned	-	M
P3	Combined	25.0%	HM
P4	Combined	14.8%	H
P5	Assigned	-	H
P6	Combined	36.9%	M
P7	Assigned	-	H
P8	Assigned	-	ML
P9	Assigned	-	ML
P10	Assigned	-	H
P11	Combined	24.8%	HM
P12	Combined	31.5%	M
P13	Assigned	-	M
P14	Assigned	-	H

High (H), High-Medium (HM), Medium (M), Medium-Low (ML), Low (L), Low-Absent (LA) and Absent (A)
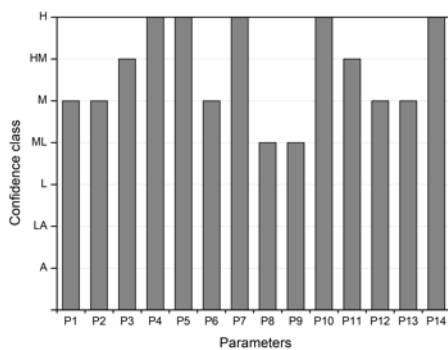

Figure 8. Bar chart distribution of the average confidence class for each parameter
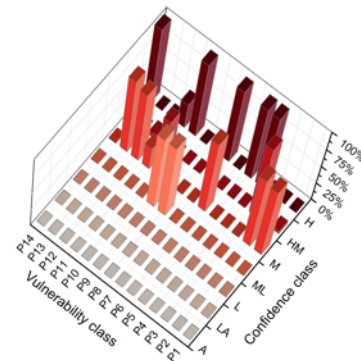
Figure 9. Matrix distribution of the confidence class for each parameter

8

225 According to these calculations, the method used for the present work takes advantage of a medium
226 confidence level with some parameters characterized by a high confidence class, generally those with a
227 directly applied class or that express only dimensional features of the buildings.

228 In conclusion, the strategies used to evaluate the uncertainties of the vulnerability index method are a
229 proposal for a starting point to include uncertainty and error propagation in large-scale vulnerability
230 assessment methods. However, the confidence level factors need an appropriate formulation based on
231 probabilistic studies that goes beyond the scope of this work. Figure 9 illustrates the distribution of the
232 uncertainties affecting this work.

5.3   Seismic vulnerability assessment

234 The vulnerability assessment described in Section 4 was applied to 153 buildings and yielded a mean
235 seismic vulnerability index value, $I_{v,mean}$, of 41.57. The minimum value of the vulnerability index was
236 16.83 and the maximum was 82.67. The associated standard deviation, σ_{1v}, is 12.93. The Kolmogorov-
237 Smirnov normality test (Frank J. Massey Jr. 1951) confirmed that at the 0.05 significance level, the data
238 was significantly drawn from a normally distributed population with a p-value of 0.148. Figure 10 shows
239 the histogram and the best-fit normal distribution curve resulting from the assessment. The buildings'
240 conservation status ranges from good condition to ruin, and a good distribution of the I_v values can be
241 observed in the plots in Figure 11 (a). This distribution was mapped in GIS software to show the spatial
242 relationship of the vulnerability index values in the study area (Figure 11).
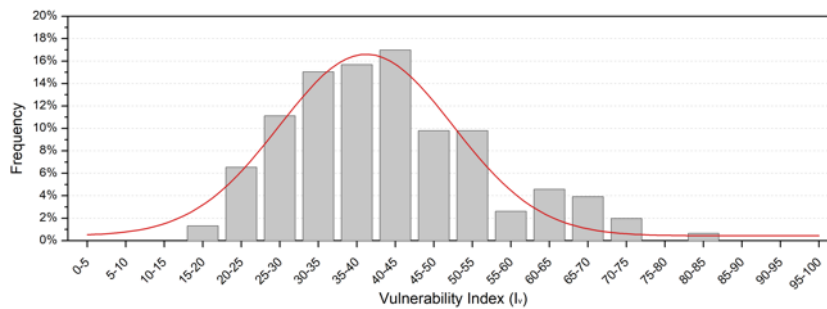
243

Figure 10. Vulnerability Index distribution of the building stock: histogram and best-fit normal distribution curve

244 The reliability of the method is demonstrated by the correlation between the most vulnerable buildings
245 identified by visual inspection (P13) and those with high I_v values. The corner and row end buildings
246 are generally more vulnerable than those located in the middle of the block, a phenomenon observed by
247 Vicente et al. (2015) and demonstrated by Figure 11. This is due to the aggregate position effect and the
248 interaction with adjacent buildings during a seismic event that may cause additional damage through the
249 floor hammering or roof misalignments.

250

9
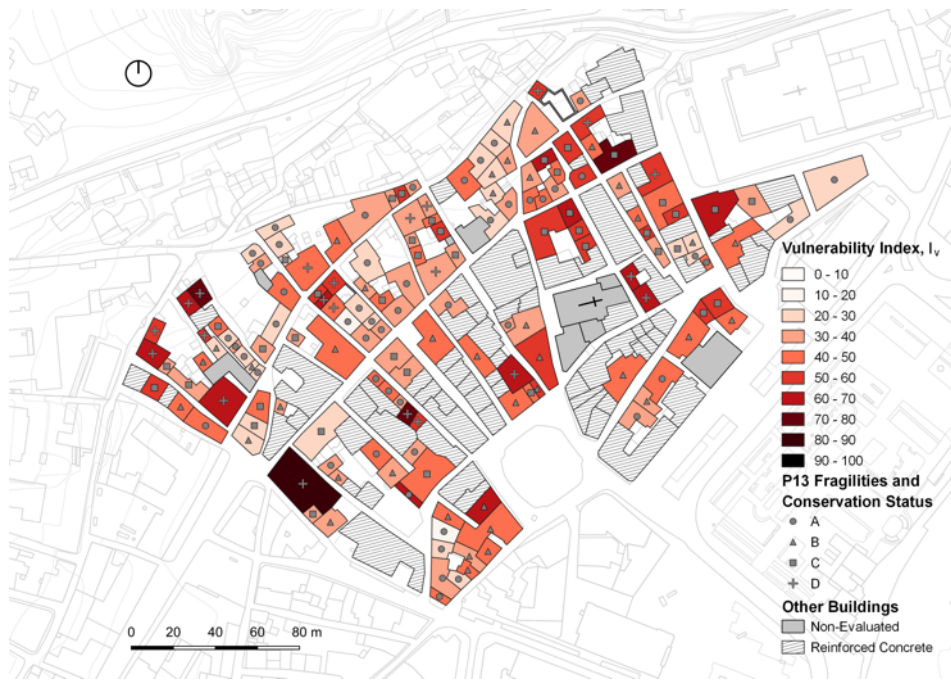
(a)
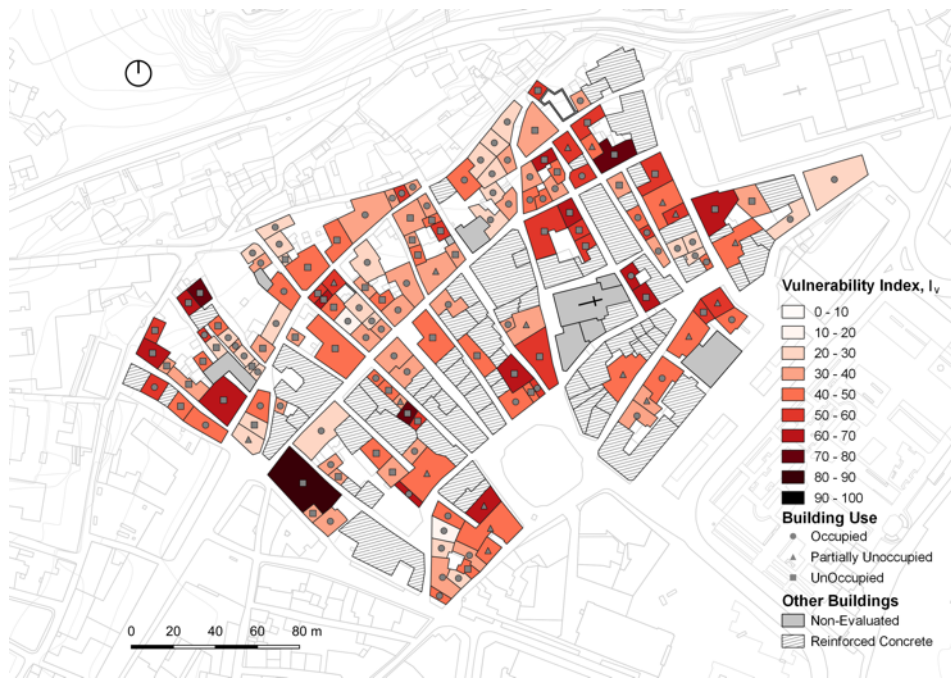
(b)

251   Figure 11. Vulnerability index values shown with: (a) class distribution of parameter P13, fragilities and conservation status;
252   and (b) state of use of buildings.

253

254   Additionally, Figure 11 (b) shows that unoccupied or partially occupied buildings generally have
255   higher vulnerability index values than occupied ones. This is due to lack of maintenance resulting
256   from the state of abandonment.

10

257 **5.4   Damage grade distributions**

258 **5.4.1   Mean damage grades**

259 In an effort to quantify the damage likely to by incurred by buildings in the historic city center of Leiria
260 for a seismic event of a given intensity, mean damage grades (μ_D) were calculated in accordance with
261 the approach proposed by Bernardini et al. with the macroseismic intensities defined by EMS - 98
262 (Bernardini et al. 2007; Grünthal 1998). The damage grades are calculated using the seismic hazard in
263 terms of the macroseismic intensity, the vulnerability index, see Equation (1), and a ductility factor
264 corresponding to the building typology according to Equation (2):

$$\mu_D = 2.5 + \left[3 \times tanh\left(\frac{I + 6.25 \times V - 12.7}{Q} \right) \right] \times f(V,I); \ 0 \leq \mu_D \leq 5 \quad (2)$$

265 where I is the seismic hazard according to EMS-98, V is the vulnerability index, and Q is the ductility
266 factor. Bernardini et al. (2007) found that the ductility factor of $Q = 3.0$ was acceptable for masonry
267 buildings similar to those found in Leiria, so the same factor was adopted for this case study. The
268 calculated damage grades range from 0 to 5, where 5 represents the worst possible damage grade.

269 Equation (3) relates the vulnerability index (I_v) described in Section 5.2 to the vulnerability index (V)
270 used in the macroseismic method and in determining the mean damage grades, and $f(V,I)$ is a function
271 of the vulnerability and intensity that pertains to trends associated with lower vulnerability grades (I$_{EMS-}$
272 $_{98}$ = V or VI), see Equation (4) (Vicente et al. 2011).

$$V = 0.592 + 0.0057 \times I_v \quad (3)$$

$$f(V,I) = \begin{cases} e^{V/2 \times (I-7)} & I \leq 7 \\ 1 & I > 7 \end{cases} \quad (4)$$

273 Vulnerability curves are plotted in Figure 12 that show the expected mean damage grade for events with
274 a range of macroseismic intensities given the mean value of the vulnerability index ($I_{v,mean}$) and upper
275 and lower bound ranges ($I_{v,mean} \pm 1\sigma_{I_v}$, $I_{v,mean} \pm 2\sigma_{I_v}$) found for Leiria.
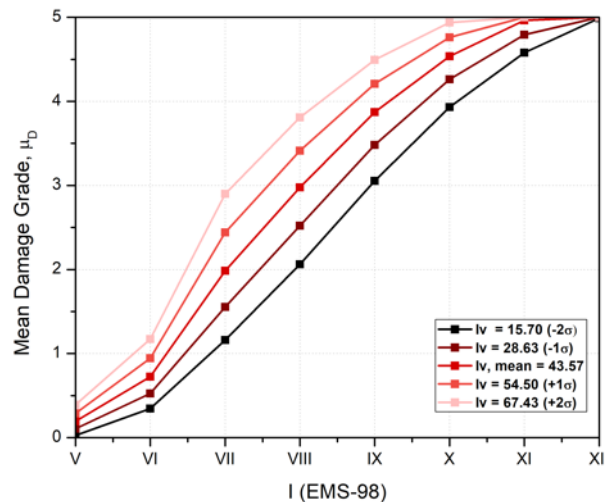

Figure 12. Mean damage grade curves for characteristic values of the vulnerability index

276

277 While the vulnerability curve is able to show the mean damage grade for the average ($I_{v,mean}$) building
278 found in Leiria's city center, by using the GIS tool the mean damage grades for every building can be

279 visualized in their actual location on the map. Figure 13 shows the distribution of the mean damage
280 grades across the study area given macroseismic intensities of VII and VIII.

(a)   (b)

281 Figure 13. Mean damage grade maps for a seismic event of Intensity I_{EMS-98} = VII (a) and I_{EMS-98} = VIII (b)

282

5.4.2 Discrete damage grades

284 The mean damage grades calculated for each building can be converted to discrete damage grades (D_k,
285 $k \in [0; 5]$) defined in EMS - 98 (Grünthal 1998). The discrete damage grade represents the cost of
286 returning a building to its original condition before the earthquake occurred. To perform the conversion
287 a probabilistic distribution based on the discretization of a beta distribution defined between 0 and 5 is
288 assumed. The correlation proposed by Bramerini et al. (1995), which can be approximated by the
289 Equation (5), was used in this case study. Damage factors (DF) defined for each discrete damage grade
290 are used to relate the discrete damage grade to the mean damage grade according to the approach
291 proposed by Maio et al. (2019).

$$\mu_D = 5\, DF^{0.52} \tag{5}$$

292 These discrete damage grades can be applied to the vulnerability indices in order to calculate fragility
293 curves and estimations of loss to describe the effect of seismic action on the historical center of Leiria,
294 which are presented in the following sections.

295

5.5 Fragility curves

297 Fragility curves can be plotted in order to visualize the probability of reaching or exceeding the discrete
298 damage grades described in the previous section for a range of macroseismic intensities. A beta
299 cumulative density function is used to define the cumulative probability of reaching or exceeding a
300 certain damage state based on the damage recorded in the database (Giovanizzi 2005).The discrete
301 probability, $P(D_k) = d$, can be derived from the difference of cumulative probabilities, $P_D[D_i \geq d]$,
302 and is described by the following Equation (6) (Ferreira et al. 2013):

$$P(D_k = d) = P_D[D_k \geq d] - P_D[D_{k+1} \geq d] \tag{6}$$

303

304 Figure 14 shows the fragility curves plotted as continuous probability functions for the mean
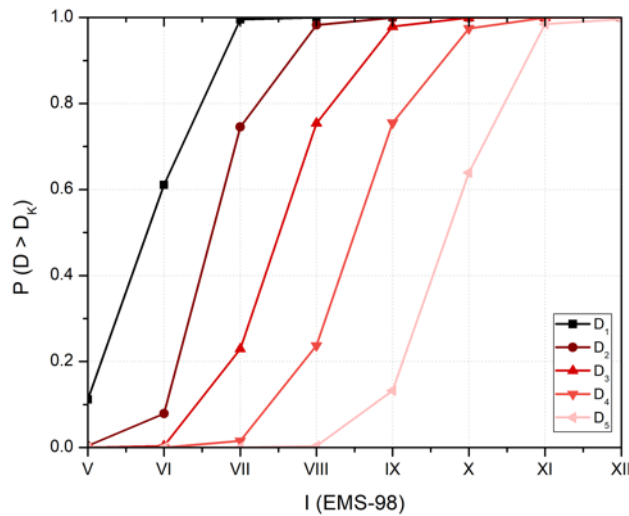305 vulnerability index value ($I_{v,mean}$ = 41.57).

12

Figure 14. Fragility curve depicting the probability of reaching or exceeding discrete damage grades D_1- D_5

306

6   Retrofitting strategies

308 The analysis shows that structural deficiencies and deterioration processes are the factors having the
309 most influence over the final I_v value. The potential vulnerabilities should be corrected by performing
310 minimum interventions that respect historical and cultural values, and economic efficiency. Although
311 interventions should be based on an assessment of a particular structure, the "packaging" strategy has
312 been recognized as an effective method for improving the seismic performance of unreinforced stone
313 masonry buildings at an urban scale (Bothara and Brzev 2011; Penna 2014; Tomaževič 1999). In the
314 present study, five retrofitting solutions for increasing invasiveness and cost, S1 to S5, are proposed and
315 grouped into two incremental packages: RP1 and RP2 (Figure 15). They are based on design
316 recommendations from the Civil Engineering Regional Laboratory of Azores (LREC) in cooperation
317 with professionals and technicians made after the 1998 earthquake (Cansado et al. 1998; Costa et al.
318 2008; Oliveira et al. 1990). The cost evaluation refers to the retrofitting strategies already proposed by
319 Ferreira et al. (2017b), based on the detailed structural design projects contained in a database related to
320 the rehabilitation process of the Faial island in 1998 which were considered representative of the
321 traditional Azorean buildings.

322 The first retrofitting package, RP1, has an estimated cost of 35 €/m², referring to the Ferreira et al. (2017
323 b) prediction, and consists of four interventions aimed at improving: wall-to-wall connection by tie-rods
324 applied at floor or roof level (S1), in-plane stiffness of diaphragms through the application of diagonal
325 bracings and new layer of timber planks (S2), wall-to-floor connection by perimeter steel beams
326 properly anchored to the stone masonry walls (S3), and wall-to-roof connection by means of tie-rods
327 that correct any potential horizontal thrust (S4). The second package RP2 has an estimated cost of 185
328 €/m² and includes all the retrofitting solutions of RP1 complemented by the jacketing technique of
329 applying a reinforced plaster layer connected to the existing masonry walls by transversal tying (S5). A
330 detailed description of each intervention is given by Ferreira *et al.* (2017b), Cansado *et al.* (1998), Costa
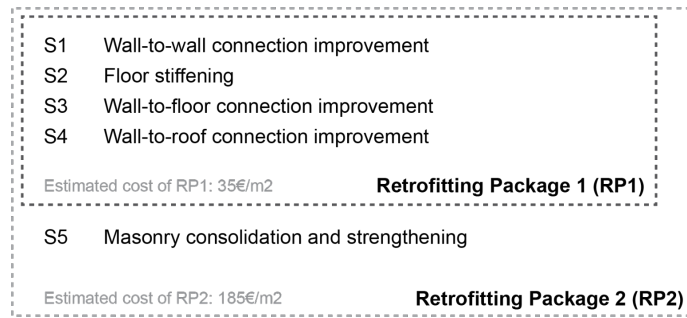331 (2002) and Bothara and Brzev (2011).

13

Figure 15. Seismic retrofitting solutions adopted

332

6.1 Vulnerability index updating

334 The effectiveness of the application of a certain retrofitting package was evaluated by updating the
335 vulnerability index values according to the parameters affected by the retrofitting technique. RP1 and
336 RP2 decrease the vulnerability index values I_v by upgrading the vulnerability classes C_{vi} of parameters
337 P1, P11, P12 and P2, P3, P13 respectively (Table 4). The application of RP1 yields a maximum
338 improvement to vulnerability class B for P1, since class A relates to designed masonry structures, and
339 to class A for P11. In the present case, parameter P12 is not upgraded because its evaluation depends on
340 expert assumptions that led to the maximum class A by default. The buildings that are grouped in the
341 lower classes have other deficiencies and thus improving the class may not be conservative.

342   Table 4. Influence of each retrofitting solution over the vulnerability index value I_v

Retrofitting solution	P1	P2	P3	P11	P12	P13
S1	✓					
S2	✓			✓		
S3	✓			✓		
S4	✓				✓	
S5	✓	✓	✓			✓
Maximum class	B	A	τ	A	-	A

343

344 The jacketing technique in RP2 influences the vulnerability class of P2, which improves to class A after
345 the intervention (Table 4). The conventional shear strength of masonry walls (P3) is updated as well.
346 Since the types and qualities of masonry walls are characterized and compared with those in the Italian
347 code, its method is applied. It allows an increase of the mechanical properties of masonry subjected to
348 intervention by multiplying them with coefficients (Circolare 21 gennaio 2019 n. 7 C.S.LL.PP. 2019).
349 Thus, the vulnerability class of P3 is updated considering the modified shear strength. The
350 implementation of both RP1 and RP2 improve the global conservation state leading to the maximum
351 class A for P13, Table 4.

352 Unlike past case studies (Ferreira et al. 2017b), the retrofitting strategies of this work were not applied
353 to the whole building stock of Leiria's city center but only to the most vulnerable building, which are
354 those with a mean damage grade above 3 for an event of macroseismic intensity VIII, which is
355 representative of the seismic hazard in Leiria. This approach is preferable because of its economic
356 affordability and because it requires minimum intervention with an acceptable degree of efficiency. As

14

a result, 69 constructions (45%) were subjected to RP1, Figure 16 (a). The updated mean damage grade
was still higher than 3 after the RP1 interventions for 21 buildings (13.7%) out of the original 69. RP2
was therefore applied to these 21 buildings to further reduce their mean damage grades, Figure 16 (b).
Finally, the total cost for the application of RP1 was computed as € 862,330.70 and the total cost for the
application of RP2 was found to be € 1,215,111.00. Bearing in mind that the given amounts are
representative and do not correspond to the real expenses that incurred by application, these results are
useful to evaluate the cost-benefit balance that will be discussed in the following sections.

(a)   (b)

Figure 16. Location of the building intervened with the RP1 (a) and the RP2 (b)

In Figure 17 the highlighted parameters are those affected by the application of each retrofitting package.
Table 5 shows the mean vulnerability index I_v and standard deviation σ_{1v} before (BR) and after (RP1
and RP2) retrofitting. Through the application of RP1, the initial mean value of seismic vulnerability
index, I_v, decreases from 41.57 to 34.05 (18.1%). Finally, by applying RP2, this reduction increases
around 26.7%. Figure 18 shows RP1 and RP2 best-fit normal distribution curves shifted and shrunk
around the updated mean I_v values as a result of the reduction in the mean vulnerability index and
standard deviation values, Table 5.

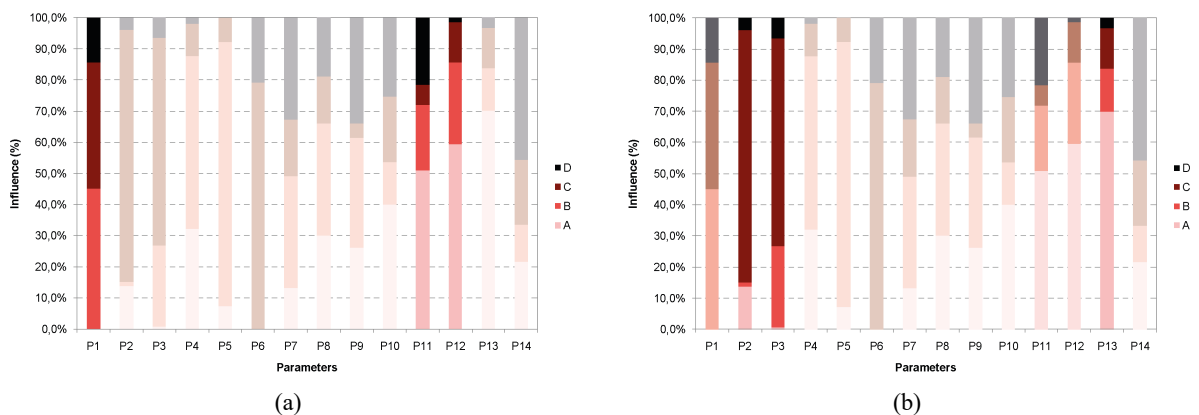(a)   (b)

Figure 17. Vulnerability class distribution after the application of RP1 to the selected 69 buildings (a) and of the RP2 to the
selected 21 buildings (b)

15

Table 5. Influence of each retrofitting solution over the I_v and standard deviation σ_{Iv}

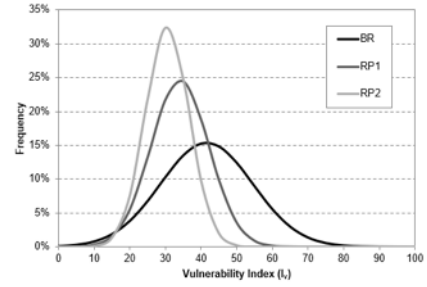| Building condition	$I_{v, mean}$	$I_{v, mean}$ reduction	σ_{Iv}	σ_{Iv} reduction
BR	41.57	-	12.93	-
RP1	34.05	18.1%	8.11	37.3%
RP2	30.49	26.7%	6.14	52.5%

Figure 18. Best-fit normal distribution curve of Iv before and after retrofitting

375

7 Loss estimation

Loss estimation has the potential to play a key role in effective loss mitigation by applying retrofitting strategies. A cost-benefit analysis based on quantitative data about the population and building stock vulnerability allows municipalities to make informed decisions regarding risk prevention (D'ayala et al. 1997) as well as the type and the extent of retrofitting strategies to adopt. Moreover, a cost-benefit analysis based on loss estimation allows for evaluation of the effectiveness of the measures taken.

Estimations of loss were calculated based on three different scenarios: before retrofitting (BR), after the application of the Retrofitting Package 1 (RP1), and after the application of the Retrofitting Package 2 (RP2). The literature presents many strategies for loss estimations based on the probabilities of occurrence of certain damage scenarios. For this approach, the loss will be estimated through the use of the characteristic vulnerability indices (I_v, $I_{v,mean} \pm 1\sigma_{I_v}$, $I_{v,mean} \pm 2\sigma_{I_v}$) and the GIS tool.

The effectiveness of the damage estimation models ultimately relies on the accuracy of the damage grades presented in Section 5.4.2. Thus, it is dependent on the probability of meeting or exceeding a certain damage grade and other loss phenomena (i.e., collapse, homelessness, death and severe injury, etc.) (Ferreira 2010).

7.1 Collapsed and unusable buildings

The estimation of probable losses in terms of collapsed and unusable buildings were calculated following the approach proposed by Bramerini et al. (1995) and adopted by the Italian *Servizio Sismico Nazionale* (SSN). The probability of a building to meet or exceed a certain damage grade is statistically weighted and summed to obtain the probabilities of collapse (Equation (7)) and unusability (Equation (8)), where the weighting factors applied were taken from values found in similar Portuguese case studies (Ferreira et al. 2013).

$$P_{collapse} = P(D_5) \qquad (7)$$

$$P_{unusable} = P(D_3) \times W_{ei,3} + P(D_4) \times W_{ei,4} \qquad (8)$$

According to the average vulnerability index values, the probability curves for collapsed and unusable buildings can be plotted for the BR scenario. Figure 19 (b) demonstrates that with increasing size of seismic events, the number of unusable buildings increases up to a maximum and then begins to decrease as the increase in the number of collapsed buildings continues to increase, Figure 19 (a). Using the GIS tool, these results can be visualized across the study area by plotting each calculated probability with the associated building code. Figure 20 (a) and (b) show the probability of unusability across the historical center of Leiria combined with the probability of collapse.

16

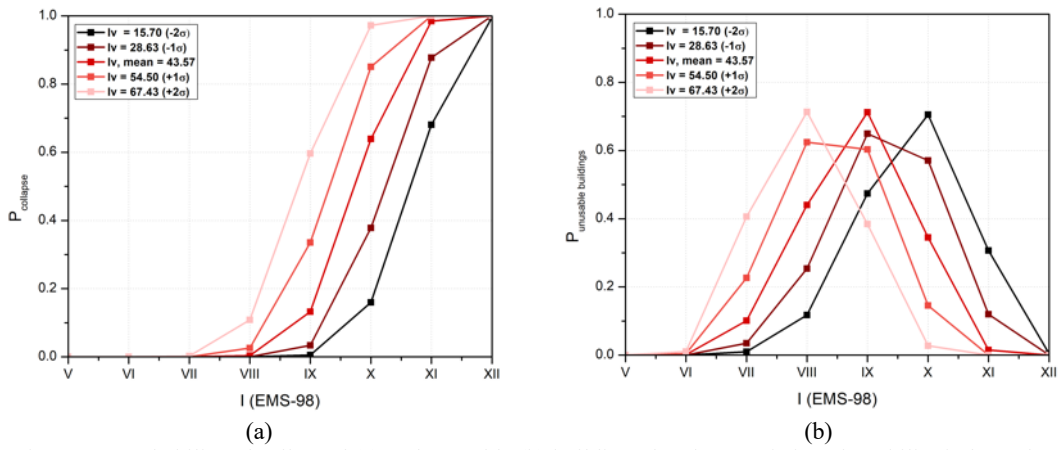(a)   (b)
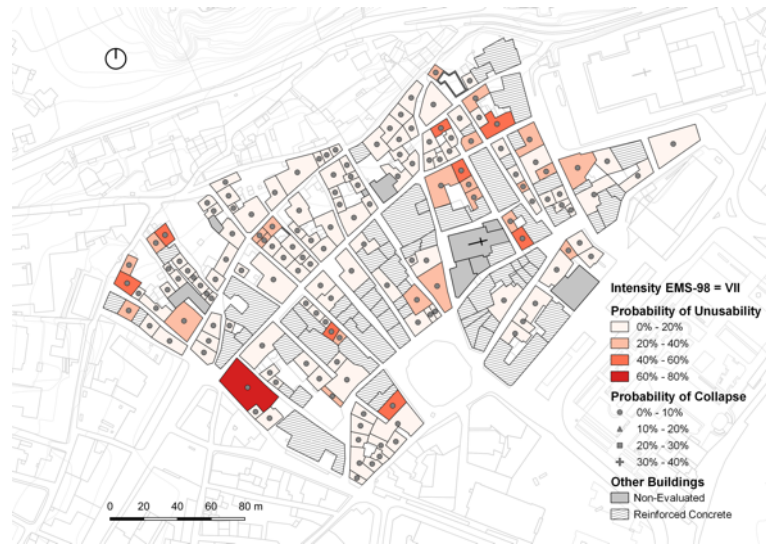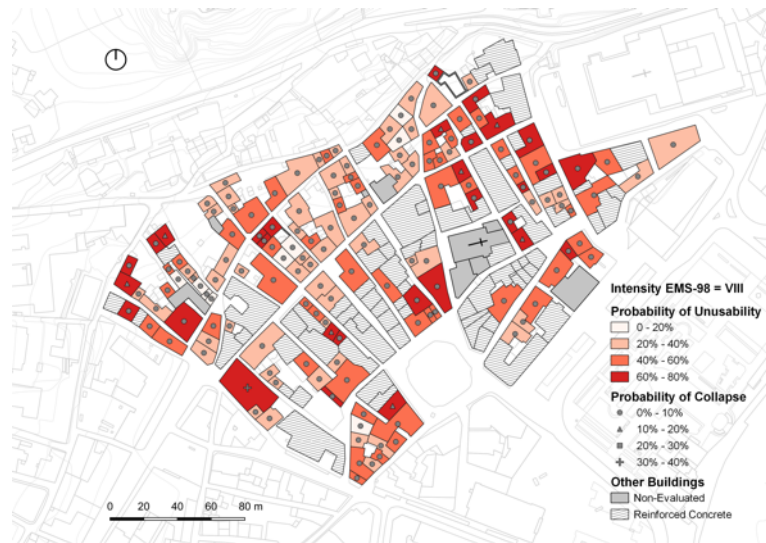
Figure 19. Probability of collapsed (a) and unusable (b) buildings for characteristic vulnerability index values

(a)

(b)

Figure 20. Map of the probabilities of unusability and collapse for an event of seismic intensity I_{EMS-98} = VII (a) and I_{EMS-98} = VIII (b)

407 The number of collapsed buildings becomes relevant when the earthquake intensity exceeds XI, which
408 is larger than expected in Leiria. However, this number can be reduced by 50% with the application of
409 the RP1 and by over 70% for RP2. The number of unusable buildings undergoes a smaller improvement
410 after retrofitting but is relevant for lower intensities. The number of unusable buildings after the
411 application of the retrofitting techniques exhibits a maximum improvement for intensity VIII (Figure
412 21) and, after reaching the peak value becomes larger than in the unreinforced condition (BR) because
413 the reinforcement strategy prevents more buildings from collapsing. In the unlikely occurrence of a
414 seismic event with intensity greater than IX, more buildings are unusable in the strengthened scenarios
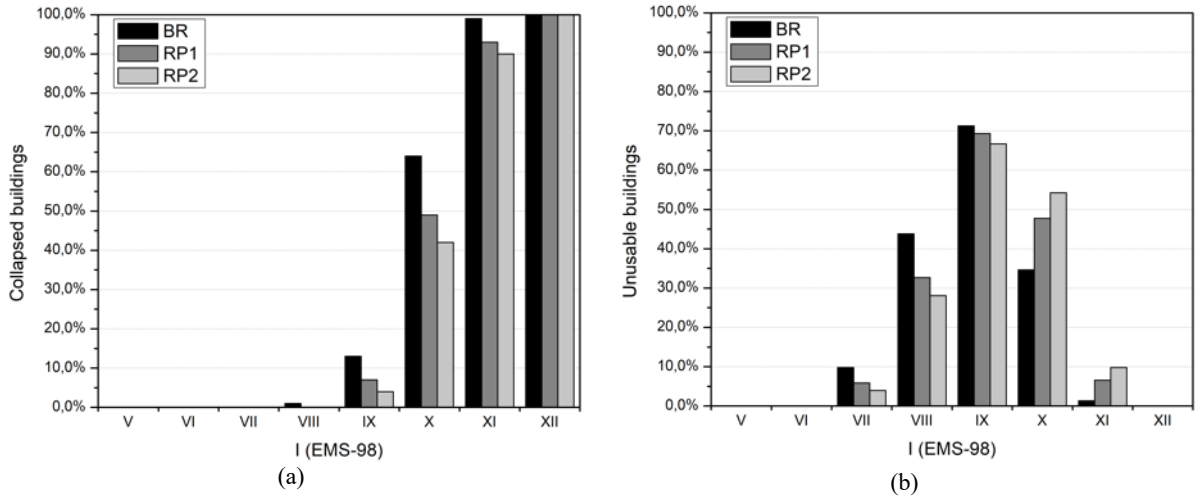415 and fewer collapse.

Figure 21. Probability of collapsed buildings (a) and unusable buildings (b) for the different building conditions analyzed

416

7.2 Human casualties

418 The approach from SSN was also used to evaluate probabilities of human casualties (dead or severely
419 injured) and homelessness in Leiria following a seismic event. Ferreira et al. (2013) defines the rate of
420 casualty as 30% of the residents in collapsed or unusable buildings, and the remaining residents of these
421 buildings as homeless. The following Equations (9) and (10) were used to determine the probabilities
422 associated with casualties and homelessness (Ferreira et al. 2013):

$$P_{death} = 0.3 \times P(D_5) \tag{9}$$

$$P_{homeless} = P(D_3) \times W_{ei,3} + P(D_4) \times W_{ei,4} + 0.7 \times D_5 \tag{10}$$

423 An estimation of the number of resulting casualties and homeless people can be calculated according to
424 the demographic data given by the census (Section 2.1) (Table 6 and Table 7). Figure 22 plots the
425 probabilities of casualties and homeless people for the characteristic vulnerability index values (I_v,
426 $I_{v,mean} \pm 1\sigma_{I_v}$, $I_{v,mean} \pm 2\sigma_{I_v}$) in the BR condition. At lower intensity events, the population is scarcely
427 affected by the earthquake in terms of deaths or injuries. Above intensity IX, the entire population falls
428 into one of these two categories, reaching a probability of 28-35% of human casualties and 70-80% of
429 homeless people. Figure 22 (b) shows the probability of homelessness reaches a maximum of about 80%
430 of the population and then decreases as the death toll arises.

18

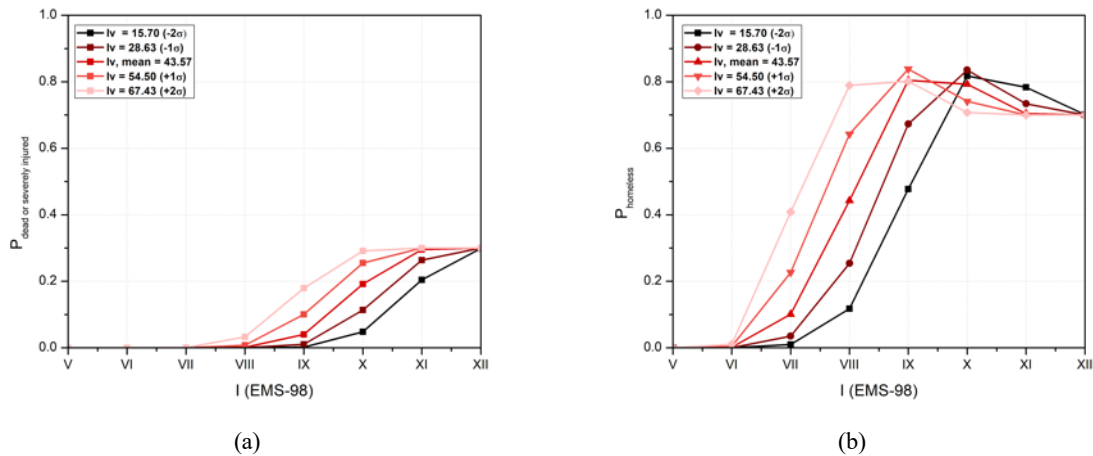| | (a) | | (b) |
| (a) | (b) |

Figure 22. Probabilities of human casualties (a) and homeless (b) for the characteristic vulnerability index values over a range of seismic intensities

431

Table 6. Estimation of the number of dead or severely injured people

	Intensity, I_{EMS-98}							
	V	VI	VII	VIII	IX	X	XI	XII
BR	0	0	0	0	13 (4.1%)	60 (19.0%)	93 (29.5%)	94 (29.8%)
RP1	0	0	0	0	6 (1.9%)	46 (14.6%)	88 (27.9%)	94 (29.8%)
RP2	0	0	0	0	4 (1.3%)	39 (12.4%)	85 (27.0%)	94 (29.8%)

432

433

Table 7. Estimation of the number of homeless people

	Intensity, I_{EMS-98}							
	V	VI	VII	VIII	IX	X	XI	XII
BR	0	0	32 (10.2%)	139 (44.1%)	254 (80.6%)	250 (79.4%)	222 (70.5%)	221 (70.2%)
RP1	0	0	18 (5.7%)	103 (32.7%)	233 (74.0%)	259 (82.2%)	226 (71.7%)	221 (70.2%)
RP2	0	0	13 (4.1%)	88 (27.9%)	220 (69.8%)	262 (83.2%)	229 (72.7%)	221 (70.2%)

434

435 Figure 23 demonstrates the effectiveness application of the retrofitting strategies on the human
436 casualties. Due to the small number of people registered as living in the city center, a probability of
437 having casualties (Figure 23 (a)) occurs only above intensity IX. However, if the maximum intensities
438 (from IX to XII) are considered, a decreasing trend can be seen after applying the RP1 and RP2 up to
439 intensity XI. After that the probability remains constant (30% for intensity XII) due to the
440 destructiveness of the seismic event. The maximum variation can be observed for intensity X where the
441 probability drops from 19% (BR) to 15% (RP1) and 12% (RP2). In terms of probability of homelessness,
442 in Figure 23 (b), a decreasing trend can be seen up to seismic intensity IX due to a decrease in the
443 number of collapsed buildings for the retrofitted scenarios. Then this trend reverses because there are
444 more non-collapsed buildings after the retrofitting interventions. These outputs can be used for
445 emergency planning by authorities and civil protection since they provide an estimation of the number
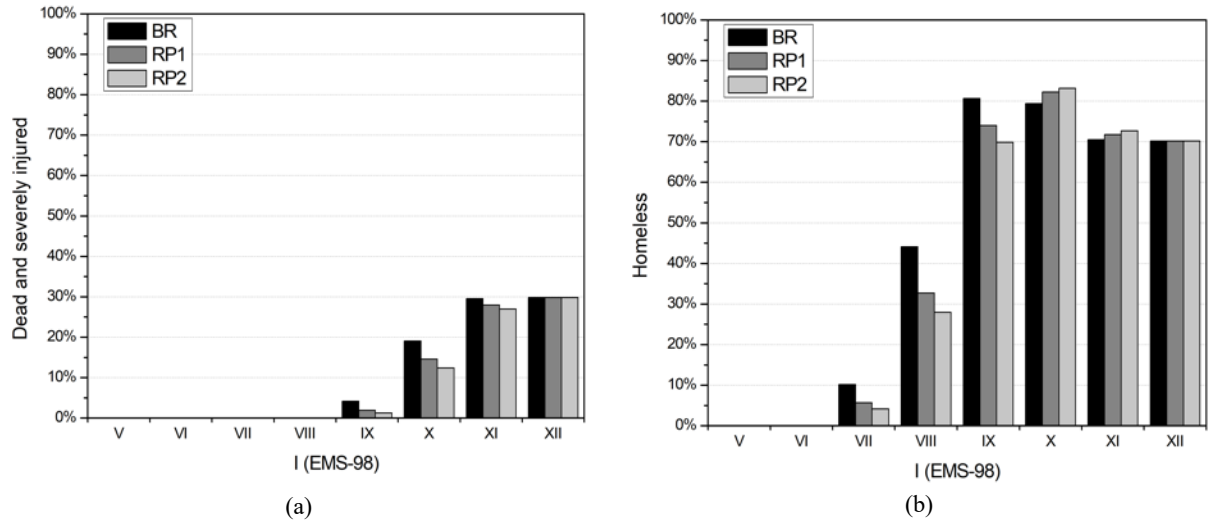446 of people that will need to be temporarily relocated.

19

Figure 23. Probability of dead or severely injured (a) and homeless (b) people

7.3 Economic balance

The estimated damage is defined as the cost of repair required for a building following a seismic event. By analyzing post-earthquake damage data and current construction costs it is possible to correlate the costs of repairs with the damage grades. This work uses the correlation developed by Maio et al. (2019) in accordance with the damage observed in 1395 buildings due to the 1998 Azores earthquake. The cost of repair and replacement is correlated to the discrete damage grades with Equation (11) proposed by Ferreira et al. (2013) using the macro-seismic intensity (I), discrete damage level ($P[R|D_k]$) and the probability of reaching that damage condition given a certain vulnerability index ($P[D_k|I_v]$).

$$P[R|I] = \sum_{D_k = 1}^{5} \sum_{I_v = 0}^{100} P[R|D_k] \times P[D_k|I_v] \tag{11}$$

While retrofitting an existing building may involve two or three times the initial investment of construction, repair and strengthening the same building after a seismic event may be four to eight times as expensive (Ferreira et al. 2017b). Moreover, the replacement of damaged or existing unsafe buildings by reconstruction should generally be avoided because of higher costs of reconstruction than those of strengthening or retrofitting actions, preservation and safeguarding of historical architecture and built heritage, and maintaining of functional, social and cultural environment (Ferreira et al. 2017b).

The economic losses are calculated singularly for each building and then summed (Table 8). In contrast, past studies have computed economic losses with respect to a mean vulnerability index value and total evaluated area of the building stock, likewise for the human losses and collapsed buildings (Ferreira et al. 2017b). The approach undertaken in this work can be considered valuable as the evaluation of economic loss for each building was possible. The economic balance can be considered the most powerful tool for evaluating the effectiveness of the retrofitting strategies considered, since it allows estimation of both the total savings obtained in terms of repair costs and replacement after a seismic event of a certain intensity and the payback of the investment undertaken (Table 9).

Table 8. Global savings obtained for each retrofitting package applied (in millions of €)

Intensity, I$_{EMS-98}$

20

	V	VI	VII	VIII	IX	X	XI	XII
RP1	0.14 M€	0.52 M€	5.12 M€	9.61 M€	9.31 M€	5.75 M€	1.29 M€	-
RP2	0.20 M€	0.75 M€	6.91 M€	13.98 M€	14.24 M€	9.28 M€	2.42 M€	-

Table 9. Payback for each retrofitting packages applied (in millions of €)

	Intensity, I_{EMS-98}							
	V	VI	VII	VIII	IX	X	XI	XII
RP1	- 0.72 M€	- 0.34 M€	4.26 M€	8.75 M€	8.44 M€	4.89 M€	0.43 M€	-0.86 M€
RP2	- 2.23 M€	-1.68 M€	4.48 M€	11.55 M€	11.81 M€	6.85 M€	-0.01 M€	-2.43 M€

The application of the retrofitting strategy decreases the estimated economic losses for low intensity earthquakes (I_{EMS-98} = VII) from 13.27 M€ to 8.15 M€ for RP1 (reduction about 39%) and to 6.36 M€ for RP2 (reduction about 52%), see Figure 24. For higher intensities the repair costs of the retrofitted scenarios are equivalent to the initial repair costs of the BR situation, because these are unlikely situations, and total destruction is expected.

Considering the repair costs and the total cost of each retrofitting package, the seismic intensity range for which the application of the indicated retrofitting strategies is effective can be identified, Figure 25.
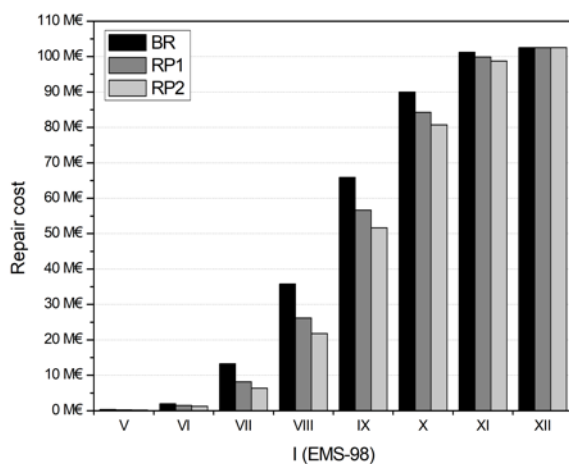

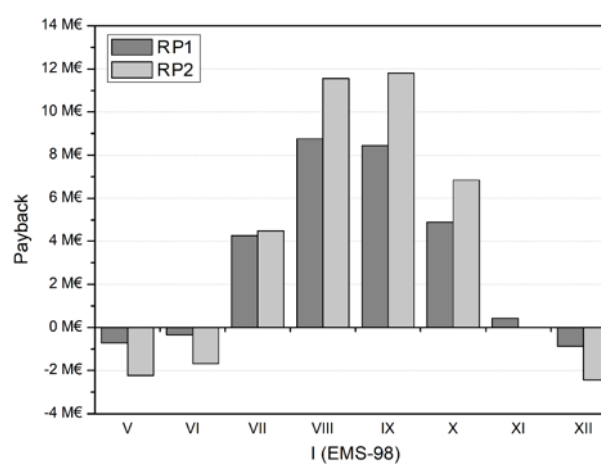Figure 24. Evaluation of the reparation costs for the different conditions analyzed

Figure 25. Evaluation of the payback amounts for the retrofitting packages applied

For low intensity earthquakes (V and VI), the initial retrofitting cost is not justified. The effectiveness range of the two intervention types are between intensities VII and X for RP1 with a payback maximum at intensity VIII of 8.75 M€ (ten times the initial investment), and for RP2 with a payback maximum at intensity IX of 11.81 € (5 times the initial investment). Beyond seismic intensity IX, the retrofitting applications start losing their effectiveness because the building stock, including the unreinforced buildings, start to suffer severe damage and collapse.

8   Conclusions

The outcomes resulting from the vulnerability assessment prove the reliability of the method proposed by Vicente et al. (2011) and Ferreira (2017a) applied to the observed characteristics and fragilities that affect structural behavior in the case of seismic events. The most vulnerable features characterizing the building stock were the connections between the various structural elements of the buildings contributing to the box-like behavior of a structure, the masonry quality, the state of conservation, and the presence of adequately stiff floor slabs that distribute and transmit the seismic load to resisting elements. Although Leiria is located in a moderate seismic hazard area, the expected level of damage for the building stock, the potential economic losses, and casualties should be reduced by means of risk management policies aimed at ensuring a sufficient seismic safety.

The hybrid method of vulnerability assessment is based on 14 different parameters that takes into account geometrical and structural characteristics, soil-structure and structure-to-structure interactions, quality of materials and construction details, conservation state. Since this method has uncertainties related to its calibration and especially to the collection of data, it is important to assess the reliability of results through a confidence factor. The strategy followed in this work allowed for the singular evaluation of the confidence class for each parameter but needs to be improved for the evaluation of a mean confidence level related to the overall vulnerability index of each building.

Bearing in mind the structural deficiencies that characterize the building stock, retrofitting strategies were aimed at mitigating seismic risk of the historical city center. The strategies properly address the most vulnerable features of the buildings in Leiria and are evaluated in a cost-benefit analysis that, through updating the vulnerability index values and computing new mean damage grades, discrete damage grades, and loss probabilities, estimates the benefits in terms of decreasing the death toll, homelessness, and collapsed and unusable buildings after a seismic event.

In conclusion, vulnerability assessment of existing structures is crucial in seismic areas to drive risk management policies and design retrofitting interventions that address observed fragilities. Through a qualitative cost-benefit analysis the evaluation of the proposed large-scale intervention allows municipalities and decision makers to make informed decisions regarding risk prevention. Interventions should be selected and designed in a way that they effectively contribute to decrease the seismic vulnerability and, in consequence, to achieve a reduction of overall damage, loss and casualty. Moreover, to be cost-efficient, the buildings to intervene (or their parts) should be wisely selected. Local authorities are able to interpret the present work on large-scale seismic analysis because its results are presented with intuitive GIS maps, thus making them aware of potential effects of their risk management policies. Moreover, outputs can be continually updated because of the integration within the GIS tool, as well as the spreadsheet database. Potential post-earthquake scenarios can be predicted for different macro-seismic intensities and their accuracy depends on the proposed calibration that takes into account the actual features of the building stock. In addition, if the results are updated with the new population data, they can provide significant information about emergency planning since the most vulnerable buildings and areas are identified, see for example (Aguado et al. 2018) and Anglade et al. (2020).

References

Aguado JLP, Ferreira TM, Lourenço PB (2018) The Use of a Large-Scale Seismic Vulnerability Assessment Approach for Masonry Façade Walls as an Effective Tool for Evaluating, Managing and Mitigating Seismic Risk in Historical Centers. *International Journal of Architectural Heritage*, 12:1259–1275. doi: 10.1080/15583058.2018.1503366

535   Anglade E, Giatreli A-M, Blyth A, et al (2020) Seismic damage scenarios for the Historic City Center of Leiria, Portugal:
536   Analysis of the impact of different seismic retrofitting strategies on emergency planning. *Internatioal Journal of Disaster*
537   *Risk Reduction,* 44:101432. doi: 10.1016/j.ijdrr.2019.101432

538   Bernardini, A., Giovinazzi, S., Lagomarsino, S., and Parodi, S. (2007). "Vulnerabilità e previsione di danno a scala territoriale
539   secondo una metodologia macrosismica coerente con la scala EMS-98." University of Canterbury. Civil and Natural
540   Resources Engineering, Pisa, Italy (in Italian).

541   Borri, A., Corradi, M., Castori, G., and De Maria, A. (2015). "A method for the analysis and classification of historic masonry."
542   *Bulletin of Earthquake Engineering*, 13(9), 2647–2665.

543   Bothara, J., and Brzev, S. (2011). *A TUTORIAL: Improving the Seismic Performance of Stone Masonry Buildings*. Svetlana
544   Brzev First Edition, July 2011.

545   Bramerini, F., Di Pasquale, G., Orsini, A., Orsini, A., Pugliese, A., Romeo, R., and Sabetta, F. (1995). "Rischio sismico del
546   territorio italiano. Proposta per una metodologia e risultati preliminari. Rapporto tecnico del Servizio Sismico National
547   SSN." (in Italian).

548   Cansado, E., Oliveira, C. S., Fragoso, M., and Miranda, V. (1998). "Regras Gerais de Reabilitação e Reconstrução de Edifícios
549   Correntes Afectados Pela Crise Sísmica do Faial, Pico e São Jorge, iniciada pelo sismo de 9 de Julho de 1998." (in
550   Portuguese).

551   Carvalho, V., and Aveleira, A. (n.d.). "Enquadramento histórico e arqueológico." <www.cm-leiria.pt/pages/405> (in
552   Portuguese).

553   Circolare 21 gennaio 2019 n. 7 C.S.LL.PP. (2019). *Circolare 21 gennaio 2019 n. 7 C.S.LL.PP. Istruzioni per l'applicazione*
554   *dell'aggiornamento delle "Norme Tecniche per le Costruzioni" di cui al D.M. 17/01/2018. Suppl. ord. alla G.U. n. 35*
555   *del 11/2/19.* (in Italian)

556   Costa, A. (2002). "Determination of mechanical properties of traditional masonry walls in dwellings of Faial Island, Azores."
557   *Earthquake Engineering and Structural Dynamics*, 31(7), 1361–1382.

558   Costa, A., Oliveira, C. S., and Neves, N. (2008). "Reinforcing Commonly More Techniques Used in Faial Reconstruction." In:
559   *Sismo 1998 – Açores. Uma Década Depois*. Sousa Oliveira, Costa & Nunes (Edt.), 531–555. ISBN: 978-989-20-1223-
560   0 (in Portuguese)

561   D'Ayala, D., Spence, R., Oliveira, C., and Pominos, A. (1997). "Earthquake Loss Estimation for Europe's Historic Town
562   Centres." *Earthquake Spectra*, 13(4), 773–793.

563   Dinis, C. (2006). *Estudo Sócio - Demográfico do Centro Histórico da Cidade de Leiria - Conclusão*. (in Portuguese)

564   Ferreira, T. M. (2010). "Avaliação da vulnerabilidade sìsmica de nùcleos urbanos antigos: Aplicação ao núcleo urbano antigo
565   do Seixal." Universidade do Porto, Portugal. (in Portuguese)

566   Ferreira, T. M., Maio, R., and Vicente, R. (2017a). "Seismic vulnerability assessment of the old city centre of Horta, Azores:
567   calibration and application of a seismic vulnerability index method." *Bulletin of Earthquake Engineering*, Springer
568   Netherlands, 15(7), 2879–2899.

569   Ferreira, T. M., Maio, R., and Vicente, R. (2017b). "Analysis of the impact of large scale seismic retrofitting strategies through
570   the application of a vulnerability-based approach on traditional masonry buildings." *Earthquake Engineering and*
571   *Engineering Vibration*, 16(2), 329–348.

572   Ferreira, T. M., Santos, C., Vicente, R., and Mendes da Silva, J. A. R. (2015). "Structural and Architectural Characterisation
573   of Old Building Stocks: Case Study of the Old City Centre of Seixal, Portugal, Rebuilt After the Great 1755 Lisbon
574   Earthquake." *Engineering Structures and Technologies*, 7(3), 126–139.

575   Ferreira, T. M., Vicente, R., Mendes da Silva, J. A. R., Varum, H., and Costa, A. (2013). "Seismic vulnerability assessment of
576   historical urban centres: case study of the old city centre in Seixal, Portugal." *Bulletin of Earthquake Engineering*, 11(5),
577   1753–1773.

578   Giovanizzi, S. (2005). "The Vulnerability Assessment and the Damage Scenario in Seismic Risk Analysis." *Chem. Ind.*, (March
579   2005).

580   GNDT. (1994). *Scheda di vulnerabilità di II livello*. Rome, Italy. (in Italian)

581   GNDT. (2003). *Manuale per la compilazione della scheda GNDT/CNR di livello II - Versione modificata dalla Regione*
582   *Toscana*. (in Italian)

583   Grünthal, G. (1998). *European Macroseismic Scale 1998 (EMS-98). Cahiers du Centre Européen de Géodynamique et de*
584   *Séismologie 15. Centre Européen de Géodynamique et de Séismologie, Luxembourg.*

585   Frank J. Massey Jr. (1951) "The Kolmogorov-Smirnov Test for Goodness of Fit", *Journal of the American Statistical*
586   *Association*, 46(253): 68–78. doi: 10.1080/01621459.1951.10500769

23

587 Maio R, Ferreira T. M., Vicente R., Costa A. (2019) Is the use of traditional seismic strengthening strategies economically
588   attractive in the renovation of urban cultural heritage assets in Portugal? *Bulletin of Earthquake Engineering* 17:2307–
589   2330. doi: 10.1007/s10518-018-00527-7

590 Maio, R., Ferreira, T. M., Vicente, R., and Estêvão, J. (2016). "Seismic vulnerability assessment of historical urban centres:
591   case study of the old city centre of Faro, Portugal." *Journal of Risk Research*, 19(5), 551–580.

592 Mattoso, J. (1985). "A cidade de Leiria na historia medieval de Portugal." *Ler historia n°4*, 2–19. (in Portuguese)

593 Oliveira, C. S., Lucas, A., and Guedes, J. H. C. (1990). *MONOGRAFIA - 10 Anos após o Sismo dos Açores de 1 de Janeiro de*
594   *1980 - Volume I e II. Secretaria Regional da Habitação e Obras Públicas, Delegação da Ilha Terceira, Açores,*
595   *Laboratório Nacional de Engenharia Civil, Angra do Heroísmo, Açores, Portugal.* (in Portuguese)

596 Penna A. (2015) Seismic assessment of existing and strengthened stone-masonry buildings: critical issues and possible
597   strategies. Bull Earthq Eng 13:1051–1071. doi: 10.1007/s10518-014-9659-0

598 Pinheiro, P., Fernandes, P., Santos, P., and Rodrigues, H. (2017). "Mechanical Characterization of Masonry Walls With Flat-
599   Jack Tests." *Nondestructive Techniques for the Assessment of Historic Structures*, CRC Press, 53–73.

600 dos Santos Gomes, T. M. (2016). "Caracterização do Parque Edificado do Centro Histórico de Leiria.". MSc Thesis. Istituto
601   Politécnico de Leiria, Portugal. (in Portuguese)

602 Teves-Costa P., Batlló J., Matias L., Catita, C., Jiménez, M. J. García-Fernández, M. (2019) Maximum intensity maps (MIM)
603   for Portugal mainland. *Journal of Seismology* 23:417–440. doi: 10.1007/s10950-019-09814-5

604 Tomaževič, M. (1999). *Earthquake-resistant Design of Masonry Buildings*. Imperial College Press, London.

605 Vicente, R. (2008). "Estratégias e metodologias para intervenções de reabilitação urbana Avaliação da vulnerabilidade e do
606   risco sísmico do edificado.". PhD Thesis. Universidade de Aveiro. (in Portuguese)

607 Vicente R., Parodi S., Lagomarsino S., Varum, H. and Mendes da Silva, J. A. R. (2011) Seismic vulnerability and risk
608   assessment: case study of the historic city centre of Coimbra, Portugal. *Bulletin of Earthquake Engineering* 9:1067–
609   1096. doi: 10.1007/s10518-010-9233-3

610 Vicente, R., Ferreira, T. M., and Mendes da Silva, J. A. R. (2015). "Supporting urban regeneration and building refurbishment.
611   Strategies for building appraisal and inspection of old building stock in city centres." *Journal of Cultural Heritage*,
612   Elsevier Masson SAS, 16(1), 1–14.

613